PHYSICAL REVIEW D **94,** 124013 (2016)

Analytic solutions of the geodesic equation for U(1)^2 dyonic rotating black holes

Kai Flathmann and Saskia Grunau

Institut für Physik, Universität Oldenburg, D–26111 Oldenburg, Germany

(Received 19 July 2016; published 9 December 2016)

In this article, we derive the geodesic equations in the U(1)^2 dyonic rotating black hole spacetime. We present their solutions in terms of the Kleinian σ function and in special cases in terms of the Weierstraß $\wp$, σ, and ζ functions. To give a list of all possible orbits, we analyze the geodesic motion of test particles and light using parametric diagrams and effective potentials.

DOI: 10.1103/PhysRevD.94.124013

I. INTRODUCTION

For many years, quantum theory and general relativity have passed all tests. Nevertheless, the unification of both theories is still an open task. One interesting development in this case is the AdS/CFT correspondence discovered in late 1997 [1]. Therefore, a conformal field theory (CFT) acting on the boundary of an anti-de Sitter (AdS) space is dual to a string theory with AdS background. Analyzing the structure of black holes in such a background could give insight into unsolved problems of the corresponding CFT. Another unsolved question is the problem of dark matter and dark energy, which possibly can be solved by introducing (pseudo)scalar fields such as dilatons and axions [2,3]. One interesting spacetime containing both fields and a nonconstant scalar potential is the dyonic rotating black hole with four electromagnetic charges of the U(1)^2 gauged supergravity found by Chow and Compère [4]. This black hole has many subcases. With pairwise equal charges and vanishing Newman-Unti-Tamburino (NUT) charge, we obtain the Kerr-Newman-AdS black hole, and the ungauged solution with four independent electromagnetic charges is given in Ref. [5]. Furthermore, by setting two of the charges equal to zero, we obtain the previously analyzed Einstein-Maxwell-dilaton-axion (EMDA) black hole solution [6].

To understand the properties of a spacetime, it is mandatory to study the geodesic behavior of test particles and light and solve the equations of motion. In this article, we derive these equations by separating the Hamilton-Jacobi equation, the separability of which can be shown by constructing Killing tensors [7,8]. This has been done for a large class of black holes in Ref. [9] and for U(1)^2 dyonic rotating black holes in Ref. [4].

Previously analytical solutions were found in terms of the Weierstraß $\wp$, σ, and ζ functions for the Schwarzschild solution [10], the Taub-NUT solution [11], the Reissner-Nordström solution [12], the five-dimensional Myers-Perry solution in the special case of equal rotation parameters [13], the Kerr-Newman spacetime for charged particles [14], the Kerr-Newman-Taub-NUT spacetime [15], and the EMDA spacetime with vanishing NUT parameter in Ref. [16], also called the Sen solution [17]. In more general cases, the solutions can be stated in terms of derivatives of the Kleinian σ functions and were used to solve the geodesic equations in the four-dimensional Schwarzschild-de Sitter [18,19] and in various higher-dimensional spacetimes like the Schwarzschild(-anti-de Sitter) and Reissner-Nordström solution [20]. The solutions were also found for the Kerr(-anti-de Sitter) spacetime [21], the higher-dimensional Myers-Perry black hole [22], and the Hořava-Lifshitz black hole [23] and in $f(R)$-gravity [24,25].

In this article, we will derive the geodesic equations in the U(1)^2 dyonic rotating black hole spacetime and present their analytical solutions in two cases: first with a vanishing gauge coupling constant or for light in terms of the Weierstraß $\wp$, σ, and ζ functions and second in terms of the hyperelliptic Kleinian σ functions. We will use parametric diagrams and effective potentials to analyze the radial and latitudinal motion and present a list of all possible orbit types afterward.

II. U(1)^2 DYONIC ROTATING BLACK HOLE

For U(1)^2 dyonic rotating black holes in asymptotically AdS coordinates, the metric is given by [4]

$$\begin{aligned} \mathrm{d}s^2 = &-\frac{R_g}{B-aA}\left(\mathrm{d}t-\frac{A}{\Xi}\mathrm{d}\phi\right)^2+\frac{B-aA}{R_g}\mathrm{d}r^2 \\ &+\frac{\Theta_g a^2\sin^2\vartheta}{B-aA}\left(\mathrm{d}t-\frac{B}{a\Xi}\mathrm{d}\phi\right)^2+\frac{B-aA}{\Theta_g}\mathrm{d}\vartheta^2, \end{aligned} \tag{1}$$

with

$$\begin{aligned} R_g &= r^2-2mr+a^2+e^2-N_g^2+g^2[r^4 \\ &\quad +(a^2+6N_g^2-2v^2)r^2+3N_g^2(a^2-N_g^2)] \\ \Theta_g &= 1-a^2g^2\cos^2\vartheta-4a^2N_g\cos\vartheta \\ A &= a\sin^2\vartheta+4N_g\sin^2\frac{\vartheta}{2} \\ B &= r^2+(N_g+a)^2-v^2 \\ \Xi &= 1-4N_gag^2-a^2g^2. \end{aligned} \tag{2}$$

Here, m is the mass parameter, a is the rotation parameter, e and v are charge dependant, N_g corresponds to the NUT

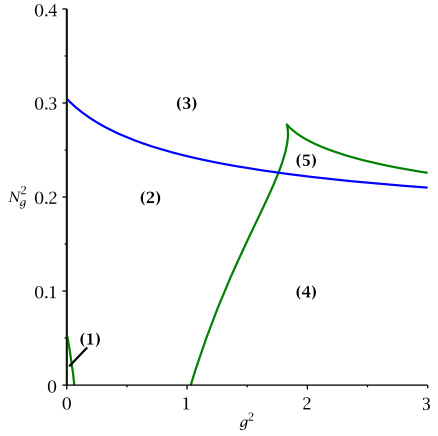

FIG. 1. Parametric $g^2 - {N_g}^2$ diagram for $a = 0.4$, $e = 0.38$, $v = 1.3$, and $m = 0.5$. The blue line represents $r = 0$ as a zero, and the green line shows where double zeros appear.

charge, and g denotes the gauge coupling constant. For further information on the parameters, see Ref. [4]. The coordinate system (t, r, ϑ, ϕ) is Boyer-Lindquist like, and the transformation to Cartesian-like coordinates reads as

$$\begin{aligned} x &= \sqrt{(r^2 + a^2)} \sin\vartheta \cos\varphi \\ y &= \sqrt{(r^2 + a^2)} \sin\vartheta \sin\varphi \\ z &= r \cos\vartheta. \end{aligned} \tag{3}$$

The horizon equation $R_g = 0$ is a polynomial equation of order 4, the solution of which can be stated analytically in the case of $g = 0$ as

$$r_\pm = m \pm \sqrt{m^2 - a^2 - e^2 + N_g^2}, \tag{4}$$

which is similar to the Kerr-Newman-Taub-NUT black hole and also, in order to have real horizons, leads to the condition $m^2 - a^2 - e^2 + N_g^2 \geq 0$ for the ungauged solution.

In the case of $g \neq 0$, the existence of four horizons, where at least one has to be negative, is possible. Here, we identify the event horizon and the Cauchy horizon from known subcases. If we want to analyze the possible zeros of R_g in general, we need to check, where double zeros appear. This leads to the condition

$$R_g(r) = 0 \quad \text{and} \quad \frac{\mathrm{d}R_g(r)}{\mathrm{d}r} = 0. \tag{5}$$

The configuration of horizons also changes, if $r = 0$ is a zero of R_g. Combining both leads to the parametric $g^2 - {N_g}^2$ diagrams in Fig. 1.

We distinguish between the following configurations:

(1) Region 1: $R_g(r)$ has only complex zeros.
(2) Region 2: Two positive zeros.
(3) Region 3: One positive and one negative zero.
(4) Region 4: Two positive and two negative zeros.
(5) Region 5: One positive and three negative zeros.

The boundary of the ergoregion exists where g_{tt} changes signs and therefore is defined by

$$a^2 \Theta_g \sin^2\vartheta - R_g = 0, \tag{6}$$

which is similar to the Kerr-Newman-Taub-NUT black hole for $g = 0$.

Because of the divergence in the Kretschmann scalar, the singularity is defined by $B - aA = r^2 + (N_g + a\cos\vartheta)^2 - v^2 = 0$. The NUT parameter N_g and the charge parameter v influence the shape of the singularity in such a way that it varies from ring singularities to three-dimensional structures in contrast to the Kerr metric, where only a ring is possible. We observed this feature in the Einstein-Maxwell-dilaton-axion spacetime [16] due to the presence of a dilaton charge at negative radial coordinate, but here these structures can also appear for a positive one. In Fig. 2, a two-dimensional projection is shown.

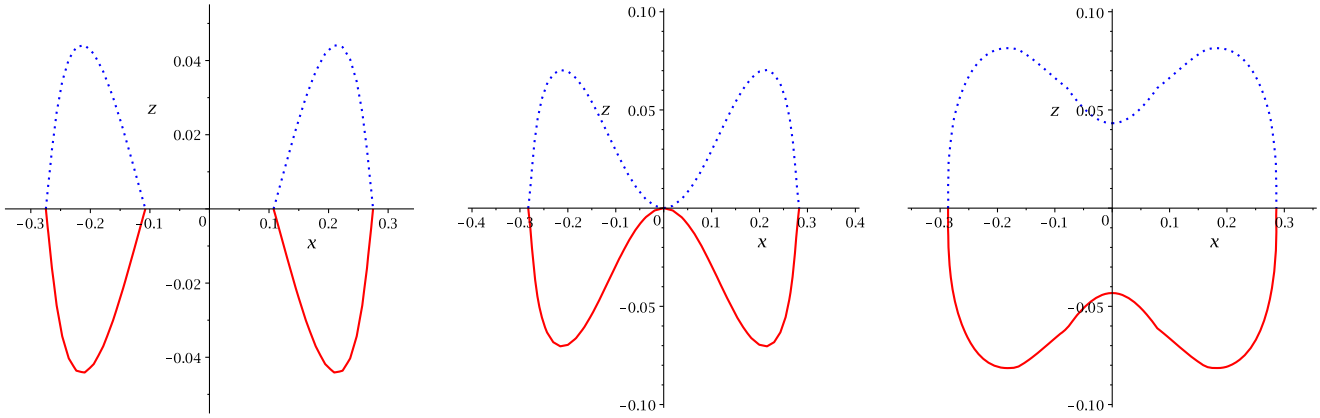

(a) $N_g = 0.2$, $a = 0.3$ and $v = 0.08$ (b) $N_g = 0.2$, $a = 0.3$ and $v = 0.1$ (c) $N_g = 0.2$, $a = 0.3$ and $v = 0.11$

FIG. 2. Plots of the singularity given by $B - aA = 0$; the dotted blue line represents $r \leq 0$, and the red line represents $r \geq 0$.

A. Geodesic equations

We use the Hamilton-Jacobi formalism to derive the geodesic equation of test particles and light. The ansatz for the action

$$S = \frac{1}{2}\delta\tau - Et + L\varphi + S_r(r) + S_\vartheta(\vartheta) \tag{7}$$

solves the Hamilton-Jacobi equation

$$\frac{\partial S}{\partial \tau} + \frac{1}{2} g^{\mu\nu} \frac{\partial S}{\partial x^\mu} \frac{\partial S}{\partial x^\nu} = 0. \tag{8}$$

Here, δ is either equal to zero for light or equal to 1 for massive particles; τ is an affine parameter along the geodesic, which corresponds to the proper time for particles; and E and L are the energy and the angular momentum of the test particle.

We obtain one differential equation for each coordinate, by separating the Hamilton-Jacobi equation (8) with the Carter [26] constant K,

$$\left(\frac{\mathrm{d}\tilde{r}}{\mathrm{d}\gamma}\right)^2 = X, \tag{9}$$

$$\sin^2\vartheta \left(\frac{\mathrm{d}\vartheta}{\mathrm{d}\gamma}\right)^2 = Y, \tag{10}$$

$$\left(\frac{\mathrm{d}\phi}{\mathrm{d}\gamma}\right) = \frac{\tilde{a}\,\tilde{\Xi}(\tilde{B}E - \tilde{a}\,\tilde{L}\,\tilde{\Xi})}{\tilde{R}} + \frac{\tilde{\Xi}(\tilde{A}E - \tilde{L}\,\tilde{\Xi})}{\tilde{\Theta}\sin^2\vartheta}, \tag{11}$$

$$\left(\frac{\mathrm{d}\tilde{t}}{\mathrm{d}\gamma}\right) = \frac{\tilde{B}(\tilde{B}E - \tilde{a}\,\tilde{L}\,\tilde{\Xi})}{\tilde{R}} + \frac{\tilde{A}(\tilde{L}\,\tilde{\Xi} - \tilde{A}E)}{\tilde{\Theta}\sin^2\vartheta}. \tag{12}$$

Here, we used dimensionless quantities

$$\begin{aligned}
&\tilde{r} = \frac{r}{2m}, \quad \tilde{t} = \frac{t}{2m}, \quad \tilde{\tau} = \frac{\tau}{2m}, \quad \tilde{N}_g = \frac{N_g}{2m},\\
&\tilde{a} = \frac{a}{2m}, \quad \tilde{g} = 2mg, \quad \tilde{e} = \frac{e}{2m}, \quad \tilde{v} = \frac{b}{2m},\\
&\tilde{K} = \frac{K}{2m}, \quad \tilde{L} = \frac{L}{2m}
\end{aligned} \tag{13}$$

and the Mino time [27] γ with $\mathrm{d}\tilde{\tau} = (\tilde{B} - \tilde{a}\,\tilde{A})\mathrm{d}\gamma$. The definition of a Mino-time simplifies the equation by absorbing the r- and ϑ-dependent prefactor $(\tilde{B} - \tilde{a}\,\tilde{A})$. We also defined the functions

$$\begin{aligned}
X &= (\tilde{B}E - \tilde{a}\,\tilde{L}\,\tilde{\Xi})^2 + \tilde{R}(\tilde{K} - \tilde{B}\delta),\\
Y &= -(\tilde{A}E - \tilde{L}\,\tilde{\Xi})^2 + \tilde{\Theta}\sin^2\vartheta(\tilde{a}\,\tilde{A}\,\delta - \tilde{K}),\\
\tilde{R} &= \tilde{r}^2 - \tilde{r} + \tilde{a}^2 + \tilde{e}^2 - \tilde{N}_g{}^2\tilde{g}^2[\tilde{r}^4 + (\tilde{a}^2 + 6\tilde{N}_g{}^2 - 2\tilde{v}^2)\tilde{r}^2\\
&\quad + 3\tilde{N}_g{}^2(\tilde{a}^2 - \tilde{N}_g{}^2)],\\
\tilde{\Theta} &= 1 - \tilde{a}^2\tilde{g}^2\cos^2\vartheta + 4\tilde{a}^2\tilde{g}^2\tilde{N}_g\cos\vartheta,\\
\tilde{A} &= \tilde{a}^2\sin^2\vartheta + 2\tilde{N}_g(1 - \cos\vartheta),\\
\tilde{B} &= \tilde{r}^2 + (\tilde{N}_g + \tilde{a})^2 - \tilde{v}^2,\\
\tilde{\Xi} &= 1 - \tilde{a}^2\tilde{g}^2 - 4\tilde{a}\,\tilde{N}_g\,\tilde{g}^2.
\end{aligned} \tag{14}$$

III. CLASSIFICATION OF THE GEODESIC MOTION

The characteristics of the geodesic motion are defined by the function Y and the polynomial X. We will study their properties with the aim of giving a full classification of the possible orbits. To obtain real values for $\tilde{r}$ and ϑ, Eqs. (9) and (10) lead to the conditions $X \geq 0$ and $Y \geq 0$. From the second condition, we derive that $\tilde{K} \geq \tilde{a}\,\tilde{A}\,\delta$ if $\tilde{\Theta} \geq 0$ and $\tilde{K} \leq \tilde{a}\,\tilde{A}\,\delta$ if $\tilde{\Theta} \leq 0$. Because of its shape, the conditions for a particle orbit that ends in the singularity can only be analyzed in special cases.

A. ϑ motion

The zeros of the function Y are the turning points of the latitudinal motion. We substitute $\nu = \cos\vartheta$ into Y and analyze the zeros in the interval $\nu = [-1, 1]$. The number of zeros changes if $\nu = 1$ or $\nu = -1$ is crossed or if Y has a double zero. The first condition $Y(\nu = 1) = 0$ is only possible if $\tilde{L} = 0$ and $Y(\nu = -1) = 0$ holds if

$$\tilde{L} = \frac{4E\tilde{N}_g}{\tilde{\Xi}}. \tag{15}$$

Double zeros appear if

$$Y(\nu) = 0 \quad \text{and} \quad \frac{\mathrm{d}Y(\nu)}{\mathrm{d}\nu} = 0. \tag{16}$$

We distinguish between four configurations (a)–(d) (compare Figs. 3 and 4):

(1) Region (a): Only negative zeros in the interval $\nu \in [-1, 1]$. The motion takes place below the equatorial plane.
(2) Region (b): Positive and negative zeros are possible in the interval $\nu \in [-1, 1]$. The motion crosses the equatorial plane.
(3) Region (c): Only positive zeros in the interval $\nu \in [-1, 1]$. The motion takes place above the equatorial plane.
(4) Region (d): No zeros in the interval $\nu \in [-1, 1]$. Geodesic motion is only possible if $Y > 0$ for all $\nu \in [-1, 1]$

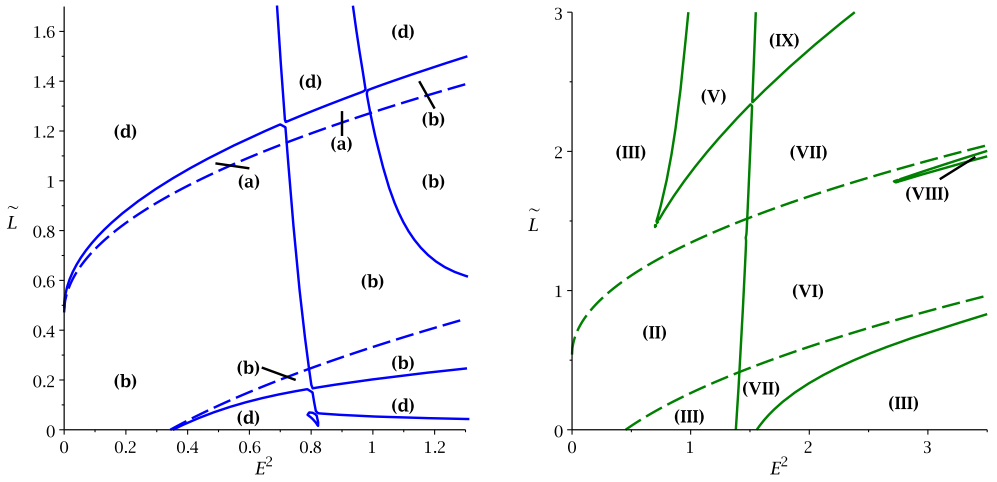

(a) ϑ-motion (b) $\tilde{r}$-motion

FIG. 3. Parametric $\tilde{L} - E^2$-diagrams for $\delta = 0$, $\tilde{a} = 0.4$, $\tilde{g} = 0.1$, $\tilde{N}_g = 0.2$, $\tilde{e} = 0.3$, $\tilde{v} = 0.2$, and $\tilde{K} = 0.1$. The continuous lines represent double zeros of $Y(\nu)$ in blue and $X(\tilde{r})$ in green. The dashed lines show zeros at $\tilde{r} = 0$ and $\nu = 0$.

The results of all conditions will be combined with the $\tilde{r}$ motion in parametric $\tilde{L} - E^2$ diagrams.

B. $\tilde{r}$ motion

First of all, let us introduce possible orbits for $r_+ > r_- > 0$,

(1) *Transit orbit* (TrO): $\tilde{r} \in (-\infty, \infty)$
(2) *Escape orbit* (EO): $\tilde{r} \in (\tilde{r}_1 > 0, \infty)$ or $\tilde{r} \in (-\infty, \tilde{r}_1)$, with $\tilde{r}_1 < 0$
(3) *Two-world escape orbit* (TEO): $\tilde{r} \in (\tilde{r}_1, \infty)$, with $0 < \tilde{r}_1 < r_-$
(4) *Crossover two-world escape orbit* (CTEO): $\tilde{r} \in (\tilde{r}_1, \infty)$, with $\tilde{r}_1 < 0$
(5) *Bound orbit* (BO): $\tilde{r} \in [\tilde{r}_1, \tilde{r}_2]$, with $\tilde{r}_1, \tilde{r}_2 > r_+$, $0 < \tilde{r}_1 < \tilde{r}_2 < r_-$ or $\tilde{r}_1, \tilde{r}_2 < 0$
(6) *Crossover bound orbit* (CBO): $\tilde{r} \in [\tilde{r}_1, \tilde{r}_2]$, with $\tilde{r}_1 < 0$ and $0 < \tilde{r}_2 < r_-$
(7) *Many-world bound orbit* (MBO): $\tilde{r} \in [\tilde{r}_1, \tilde{r}_2]$, with $0 < \tilde{r}_1 < r_-$ and $r_+ < \tilde{r}_2$
(8) *Crossover many-world bound orbit* (CMBO): $\tilde{r} \in [\tilde{r}_1, \tilde{r}_2]$, with $\tilde{r}_1 < 0$ and $r_+ < \tilde{r}_2$

We can characterize the radial motion by analyzing the zeros of the polynomial X, since these are the turning points. As for the ϑ motion, double zeros appear if

$$X(\tilde{r}) = 0 \quad \text{and} \quad \frac{\mathrm{d}X(\tilde{r})}{\mathrm{d}\tilde{r}} = 0, \tag{17}$$

and the number of positive or negative zeros changes, if one zero crosses $\tilde{r} = 0$. In Figs. 3 and 4, we show two examples of parametric $\tilde{L} - E^2$ diagrams for the ϑ and the $\tilde{r}$ motion.

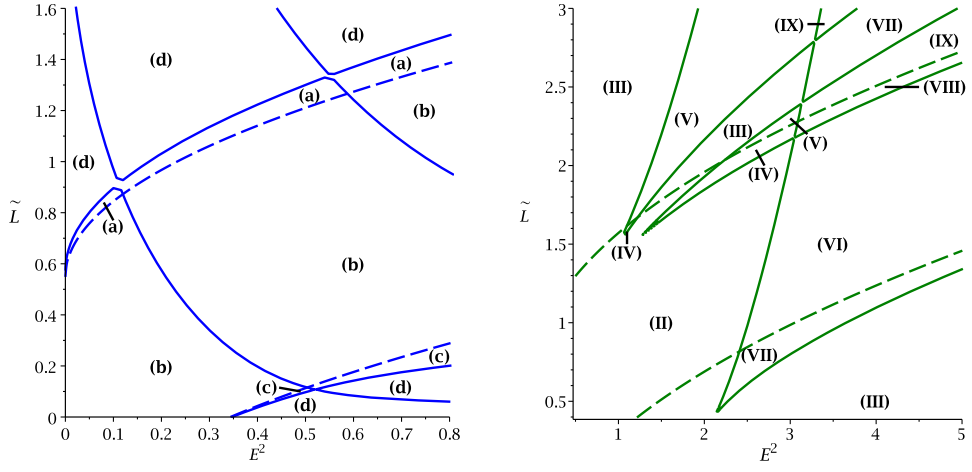

(a) ϑ-motion (b) $\tilde{r}$-motion

FIG. 4. Parametric $\tilde{L} - E^2$ diagrams for $\delta = 0$, $\tilde{a} = 0.4$, $\tilde{g} = 0.55$, $\tilde{N}_g = 0.2$, $\tilde{e} = 0.3$, $\tilde{v} = 0.2$, and $\tilde{K} = 0.1$. The continuous lines represent double zeros of $Y(\nu)$ in blue and $X(\tilde{r})$ in green. The dashed lines show zeros at $\tilde{r} = 0$ and $\nu = 0$.

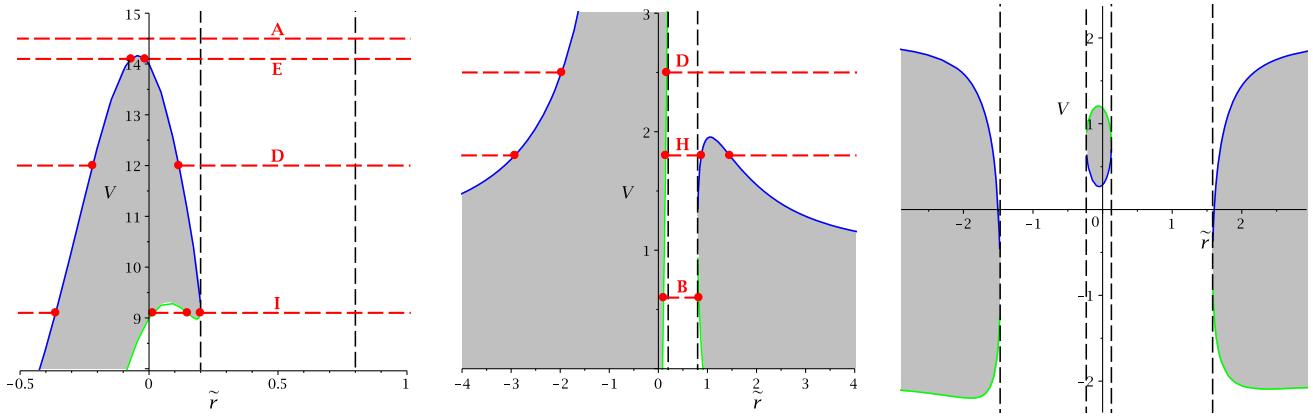

(a) $\delta = 0$, $\tilde{a} = 0.4$, $\tilde{g} = 0$, $\tilde{N_g} = 0$, $\tilde{e} = 0$, $\tilde{v} = 0$, $\tilde{K} = -1$ and $\tilde{L} = 4.6$ (b) $\delta = 1$, $\tilde{a} = 0.4$, $\tilde{g} = 0$, $\tilde{N_g} = 0$, $\tilde{e} = 0$, $\tilde{v} = 0$, $\tilde{K} = -10$ and $\tilde{L} = 2.3$ (c) $\delta = 0$, $\tilde{a} = 0.4$, $\tilde{g} = 2$, $\tilde{N_g} = \sqrt{0.1}$, $\tilde{e} = 0.38$, $\tilde{v} = 1.3$, $\tilde{K} = -1$ and $\tilde{L} = 1.3$

FIG. 5. Illustration of the effective potential $V_\pm$ and energies for examples of orbit types of Table I. The blue line represents V_+, and the green line represents V_-. The red dots denote the turning points of the particle, and the grey area forbids geodesic motion due to $X \leq 0$.

The areas in Figs. 3 and 4 are named to distinguish between configurations of the zeros of the polynomial X:

(1) Region (I): $X(\tilde{r})$ has no real zero for $\tilde{r} \in (-\infty, \infty)$. Only TrO are possible.
(2) Region (II): Two real zeros $\tilde{r}_1$ and $\tilde{r}_2$ in the interval $(-\infty, \infty)$. Here, MBO are possible.
(3) Region (III): Two real zeros $\tilde{r}_1$ and $\tilde{r}_2$ with $\tilde{r}_1 \in (-\infty, 0]$ and $\tilde{r}_1 \in [0, \infty)$. The new class of a CMBO is possible.
(4) Region (IV): Four positive real zeros exists. In this region, BO and MBO exist.
(5) Region (V): Four real zeros $\tilde{r}_1$, $\tilde{r}_2$, $\tilde{r}_3$, $\tilde{r}_4$ with $\tilde{r}_1 \in (-\infty, 0]$ and $\tilde{r}_2$, $\tilde{r}_3$, $\tilde{r}_4 \in [0, \infty)$. Here, CBO and MBO are possible.
(6) Region (VI): Two positive and two negative real zeros. Here BO and MBO exist.
(7) Region (VII): One positive and three negative real zeros. BO and MBO are possible.
(8) Region (VIII): Six real zeros $\tilde{r}_1$, $\tilde{r}_2$, $\tilde{r}_3$, $\tilde{r}_4$, $\tilde{r}_5$, $\tilde{r}_6$ with $\tilde{r}_1$, $\tilde{r}_2$, $\tilde{r}_3$, $\tilde{r}_4 \in (-\infty, 0]$ and $\tilde{r}_5$, $\tilde{r}_6 \in [0, \infty)$. Here, BO and MBO are possible.
(9) Region (IX): Three positive and three negative real zeros. Possible orbits are a BO and a CBO which could lie inside the singularity.

In addition, we can rewrite X as

$$X = f(\tilde{r})(E - V_+)(E - V_-) \tag{18}$$

to determine an effective potential $V_\pm$. Now, we can visualize the turning points of the $\tilde{r}$ motion with the intersections of E and $V_\pm$. Figures 5(a) and 5(b) show two examples of the effective potential $V_\pm$, where orbits are shown with vanishing gauge coupling constant. In Fig. 5(c), we can see that negative horizons have the same effect on the effective potential as the horizons at positive $\tilde{r}$. We assume that similar orbits are possible and only take a look at the particle motion for two positive horizons. To summarize, we present a list of all possible orbit types in Table I.

C. Comparison to previous work

Comparing the orbit types found in the $U(1)^2$ dyonic rotating black hole spacetime to previous work, we notice the following.

Common escape (EO) and bound orbits (BO), which can also cross the horizons (TEO, MBO), are present in most of the previously analyzed spacetimes, like the Kerr-(anti)-de Sitter spacetime [21], the Taub-NUT spactime [11], the Reissner-Nordström spacetime [12], the Kerr-Newman spacetime [14], the Sen black hole in Ref. [16], and many more.

Crossover orbits, which cross $\tilde{r} = 0$, can of course only be found in spacetimes where the shape of the singularity allows the geodesics to reach negative $\tilde{r}$. Unbound crossover orbits like TrOs and CTEOs exist, for example, in the Kerr-de Sitter spacetime, the Taub-NUT spactime, the Kerr-Newman spacetime, and the Sen black hole. Bound crossover orbits (CBO and CMBO) can be seen in the Kerr-AdS spacetime, the Taub-NUT spactime, and the Kerr-Newman spacetime, but not for the Sen black hole.

In the spacetime of a $U(1)^2$ dyonic rotating black hole, we find the orbit types A–L shown in Table I. The orbit types A, B, D, E, F_, G, H, and I also exist around the Sen black hole. B, F_+, and G can be seen in the Reissner-Nordström spacetime. A, B, D, E, G, H, and I are found in the Kerr spacetime. A, D, E, H, and I are also present in the Kerr dS spacetime, while C, F_+, F_-, G, J, and K are found in the Kerr AdS spacetime.

In Ref. [14], the motion of charged particles around an electrically and magnetically charged Kerr-Newman black hole was investigated. There, the structure of the orbit types is similar to the $U(1)^2$ dyonic rotating black hole, and the same orbit types A–J are present. The orbit types K and L

TABLE I. Possible types of orbits in the $U(1)^2$ dyonic rotating black hole spacetime. The thick lines represent the range of $\tilde{r}$. $\tilde{r} = 0$ is represented by blank circle, and the horizons are represented by two vertical lines. The turning points are indicated by thick dots.

Type	Zeros	Region	Range of $\tilde{r}$	Orbit
A	0			TrO
B	2	II a,b,c		MBO
C	2	III a,c		CMBO
D	2			EO, TEO
E	2			EO, CTEO
F	4	V a		CBO, MBO
F_+		IV a,b		BO, MBO
F_-		VI a,b,c		BO, MBO
G	4	IV a		MBO, BO
H	4			EO, MBO, EO
I	4			EO, BO, TEO
J	4	VII a,b,c		BO, CMBO
K	6	VIII a,b		BO, BO, MBO
L	6	IX a		BO, CBO, BO

do not exist in the Kerr-Newman spacetime since six zeros are required and the r equation in the Kerr-Newman spacetime only allows up to four zeros. It is likely that adding a negative cosmological constant to the electrically and magnetically charged Kerr-Newman black hole will produce orbits of the types K and L.

IV. SOLUTION OF THE GEODESIC EQUATIONS

In this section, we present the analytical solution of the equations (9)–(12) in two cases. The first ones are valid for vanishing gauge coupling constant $\tilde{g}$ or for light ($\delta = 0$) and are given in terms of the Weierstraß $\wp$, σ, and ζ functions. The second ones can be used for any values of the parameters but are more complicated to handle. These solutions are given in terms of the Kleinian σ function.

A. $\tilde{r}$ equation

In general, the right-hand side of (9) is an order-6 polynomial $X = \sum_{i=1}^{6} a_i \tilde{r}^i$ with the coefficients

$$
\begin{aligned}
a_6 &= -\tilde{g}^2\delta \\
a_5 &= 0 \\
a_4 &= E^2 - \delta + \tilde{g}^2[\tilde{K} + \delta(-7\tilde{N}_g{}^2 - 2\tilde{N}_g\tilde{a} - 2\tilde{a}^2 + 3\tilde{v}^2)] \\
a_3 &= \delta \\
a_2 &= 2E\tilde{L}\,\tilde{a}(4\tilde{N}_g\tilde{a}\,\tilde{g}^2 - 1) + 2E^2(\tilde{a} + \tilde{N}_g + \tilde{v})(\tilde{a} + \tilde{N}_g - \tilde{v}) \\
&\quad - \delta[((\tilde{N}_g + \tilde{a})^2 - \tilde{v}^2)(1 + \tilde{g}^2(6\tilde{N}_g{}^2 + \tilde{a}^2 - 2\tilde{v}^2)) - \tilde{N}_g{}^2 + 3\tilde{g}^2\tilde{N}_g{}^2(\tilde{a}^2 - \tilde{N}_g{}^2) + \tilde{a}^2 + \tilde{e}^2] \\
&\quad + \tilde{K}(1 + \tilde{g}^2(6\tilde{N}_g{}^2 + \tilde{a}^2 - 2\tilde{v}^2)) \\
a_1 &= \delta(\tilde{a} + \tilde{N}_g + \tilde{v})(\tilde{a} + \tilde{N}_g - \tilde{v}) - \tilde{K} \\
a_0 &= \tilde{L}^2\tilde{a}^2(4\tilde{N}_g\tilde{a}\,\tilde{g}^2 + \tilde{a}\tilde{g}^2 - 1)^2 + 8E\tilde{L}\,\tilde{a}\left(\tilde{N}_g\tilde{a}\,\tilde{g}^2 + \frac{1}{4}\tilde{a}^2\tilde{g}^2 - \frac{1}{4}\right)(\tilde{a} + \tilde{N}_g + \tilde{v})(\tilde{a} + \tilde{N}_g - \tilde{v}) \\
&\quad + ((\tilde{N}_g + \tilde{a})^2 - \tilde{v}^2)^2 - \delta(\tilde{N}_g + \tilde{a})^2 - \tilde{v}^2)(-\tilde{N}_g{}^2 + 3\tilde{g}^2\tilde{N}_g{}^2(\tilde{a}^2 - \tilde{N}_g{}^2) + \tilde{a}^2 + \tilde{e}^2) \\
&\quad + \tilde{K}(-\tilde{N}_g{}^2 + 3\tilde{g}^2\tilde{N}_g{}^2(\tilde{a}^2 - \tilde{N}_g{}^2) + \tilde{a}^2 + \tilde{e}^2).
\end{aligned}
\tag{19}
$$

1. Elliptic case

For $\tilde{g}$ or δ equal to zero, $a_6 = 0$, and therefore X is a polynomial of order 4. With the substitution $\tilde{r} = \pm\frac{1}{x} + r_X$, where r_X is a zero of X, Eq. (9) becomes

$$
\left(\frac{\mathrm{d}x}{\mathrm{d}\gamma}\right)^2 = \sum_{i=0}^{3} b_i x^i \tag{20}
$$

with fixed coefficients. With $x = \frac{1}{b_3}(4y - \frac{b_2}{3})$, Eq. (9) becomes

$$\left(\frac{\mathrm{d}y}{\mathrm{d}\gamma}\right)^2 = 4y^3 - g_2^{\tilde{r}} y - g_3^{\tilde{r}} = P_3^{\tilde{r}}(y), \tag{21}$$

with

$$g_2^{\tilde{r}} = \frac{b_2^2}{12} - \frac{b_1 b_3}{4}, \qquad g_3^{\tilde{r}} = \frac{b_1 b_2 b_3}{48} - \frac{b_0 b_3^2}{16} - \frac{b_2^3}{216}. \tag{22}$$

Equation (21) is a differential equation in the standard Weierstraß form which can be solved by [28]

$$y(\gamma) = \wp(\gamma - \gamma'_{\mathrm{in}}; g_2^{\tilde{r}}, g_3^{\tilde{r}}), \tag{23}$$

where γ'_{in} only depends on the initial value $\tilde{r}_{\mathrm{in}}$ by $\gamma'_{\mathrm{in}} = \gamma_{\mathrm{in}} + \int_{y_{\mathrm{in}}}^{\infty} \frac{\mathrm{d}y}{\sqrt{4y^3 - g_2^{\tilde{r}} y - g_3^{\tilde{r}}}}$ with $y_{\mathrm{in}} = \pm\frac{b_3}{4\tilde{r}_{\mathrm{in}}} + \frac{b_2}{12}$. With resubstitution, we can obtain the solution of Eq. (9),

$$\tilde{r} = \pm \frac{b_3}{4\wp(\gamma - \gamma'_{\mathrm{in}}; g_2^{\tilde{r}}, g_3^{\tilde{r}}) - \frac{b_2}{3}} + \tilde{r}_R. \tag{24}$$

2. Hyperelliptic case

Now, we look at Eq. (9) for nonvanishing $\tilde{g}$ and massive particles. We can transform this equation to

$$\left(x\frac{\mathrm{d}x}{\mathrm{d}\gamma}\right)^2 = \sum_{i=0}^{5} b_i x^i =: P_5^{\tilde{r}}(x) \tag{25}$$

with $\tilde{r} = \pm\frac{1}{x} + r_X$. Separation leads to

$$\gamma - \gamma_{\mathrm{in}} = \int_{x_{\mathrm{in}}}^{x} \frac{x' dx'}{\sqrt{P_5^{\tilde{r}}(x')}}. \tag{26}$$

Equation (26) contains a hyperelliptic integral of the first kind and can be solved in terms of derivatives of the Kleinian σ function,

$$x = -\frac{\sigma_1(\vec{\gamma}_\infty)}{\sigma_2(\vec{\gamma}_\infty)}, \tag{27}$$

where $\sigma_i = \frac{\partial\sigma(\vec{z})}{\partial z_i}$ and

$$\vec{\gamma}_\infty = \left(-\int_x^\infty \frac{\mathrm{d}x}{\sqrt{P_5^{\tilde{r}}(x)}}, \gamma - \gamma_{\mathrm{in}} - \int_{x_{\mathrm{in}}}^\infty \frac{x\mathrm{d}x}{\sqrt{P_5^{\tilde{r}}(x)}}\right)^T. \tag{28}$$

These methods were developed in Ref. [29]. By resubstitution, we get the full solution of (9),

$$\tilde{r}(\gamma) = \mp \frac{\sigma_2(\vec{\gamma}_\infty)}{\sigma_1(\vec{\gamma}_\infty)} + \tilde{r}_X. \tag{29}$$

B. ϑ equation

Equation (10) can be solved similarly to the $\tilde{r}$ equation (9). By introducing $\nu = \cos\vartheta$, Eq. (10) becomes

$$\left(\frac{\mathrm{d}\nu}{\mathrm{d}\gamma}\right)^2 = \sum_{i=0}^{6} a'_i \nu^i = Y_\nu(\nu) \tag{30}$$

with the coefficients

$$\begin{aligned}
a'_6 &= -\delta\tilde{g}^2\tilde{a}^4 \\
a'_5 &= -6\delta\tilde{N}_g\tilde{g}^2\tilde{a}^4 \\
a'_4 &= \delta\tilde{g}^2\tilde{a}^4 - E^2\tilde{a}^2 - \tilde{K}\tilde{a}^2\tilde{g}^2 \\
&\quad - \delta\tilde{a}(8\tilde{a}\tilde{N}_g{}^2\tilde{g}^2 - \tilde{a}^2\tilde{g}^2(\tilde{a} + 2\tilde{N}_g) - \tilde{a}) \\
a'_3 &= 6\delta\tilde{g}^2\tilde{a}^3\tilde{N}_g - 4E^2\tilde{N}_g\,\tilde{a} - 4\tilde{K}\,\tilde{N}_g\,\tilde{g}^2 \\
&\quad - \tilde{a}\delta(-4\tilde{a}\,\tilde{N}_g\,\tilde{g}^2(\tilde{a} + 2\tilde{N}_g) - 2\tilde{N}_g) \\
a'_2 &= \tilde{K}(1 + \tilde{a}^2\tilde{g}^2) + \tilde{a}\delta(8\tilde{N}_g{}^2\tilde{a}\tilde{g}^2 - \tilde{a} \\
&\quad - (\tilde{a} + 2\tilde{N}_g)(1 + \tilde{a}^2\tilde{g}^2)) \\
a'_1 &= 4\tilde{K}\,\tilde{a}\,\tilde{N}_g\,\tilde{g}^2 - \tilde{a}\delta(4\tilde{a}\,\tilde{N}_g\,\tilde{g}^2(\tilde{a} + 2\tilde{N}_g) - 2\tilde{N}_g) \\
&\quad + 4\tilde{N}_g E^2(\tilde{a} + 2\tilde{N}_g) - 4\tilde{N}_g\,\tilde{L}\,E(1 - 4\tilde{N}_g\,\tilde{a}\,\tilde{g}^2 - \tilde{a}^2\tilde{g}^2) \\
a'_0 &= \tilde{a}\delta(\tilde{a} + 2\tilde{N}_g) - \tilde{K} + (E(\tilde{a} + 2\tilde{N}_g) \\
&\quad - L(1 - 4\tilde{N}_g\,\tilde{a}\,\tilde{g}^2 + \tilde{a}^2\tilde{g}^2))^2.
\end{aligned} \tag{31}$$

1. Elliptic case

As for the $\tilde{r}$ equation (9), we can first set $\tilde{g}$ or δ to zero to get a differential equation, which can be solved by the Weierstraß $\wp$ function. The substitution $\nu = \pm\frac{1}{\mu} + \nu_Y$, where ν_Y is a zero of Y_ν, leads to the form

$$\left(\frac{\mathrm{d}\mu}{\mathrm{d}\gamma}\right)^2 = \sum_{i=0}^{3} b'_i \mu^i. \tag{32}$$

Finally, $\mu = \frac{1}{b'_3}(4\xi - \frac{b'_2}{3})$ transforms (10) into the standard Weierstraß form

$$\left(\frac{\mathrm{d}\xi}{\mathrm{d}\gamma}\right)^2 = 4\xi^3 - g_2^\vartheta\xi - g_3^\vartheta = P_3^\vartheta(\xi), \tag{33}$$

which has the solution

$$\xi(\gamma) = \wp(\gamma - \gamma''_{\mathrm{in}}; g_2^\vartheta, g_3^\vartheta), \tag{34}$$

where $\gamma''_{\mathrm{in}} = \gamma_{\mathrm{in}} + \int_{\xi_{\mathrm{in}}}^\infty \frac{\mathrm{d}\xi}{\sqrt{4\xi^3 - g_2^\vartheta\xi - g_3^\vartheta}}$ with $\xi_{\mathrm{in}} = \pm\frac{b'_3}{4\nu_{\mathrm{in}}} + \frac{b'_2}{12}$. Here, the constants are

$$g_2^\vartheta = \frac{b'_2{}^2}{12} - \frac{b'_1 b'_3}{4}, \quad g_3^\vartheta = \frac{b'_1 b'_2 b'_3}{48} - \frac{b'_0 b'_3{}^2}{16} - \frac{b'_2{}^3}{216}. \tag{35}$$

Now, we can state the solution of (10) after resubstitution as

$$\vartheta(\gamma) = \arccos\left(\frac{b'_3}{4\wp(\gamma - \gamma''_{\mathrm{in}}; g_2^\vartheta, g_3^\vartheta) - \frac{b'_2}{3}} + \nu_Y\right). \tag{36}$$

2. Hyperelliptic case

To derive the full solution of Eq. (10), we substitute $\cos\vartheta = \pm\frac{1}{\nu} + \nu_Y$ and get

$$\left(\nu\frac{\mathrm{d}\nu}{\mathrm{d}\gamma}\right)^2 = \sum_{i=0}^{5} b_i'\nu^i =: P_5^\vartheta(\nu), \tag{37}$$

the solution of which can be formulated as

$$\vartheta = \arccos\left(\mp\frac{\sigma_2(\vec{\gamma'}_\infty)}{\sigma_1(\vec{\gamma'}_\infty)} + \nu_Y\right), \tag{38}$$

with

$$\vec{\gamma'}_\infty = \left(-\int_\nu^\infty \frac{\mathrm{d}\nu}{\sqrt{P_5^\vartheta(\nu)}}, \gamma - \gamma_{\mathrm{in}} - \int_{\nu_{\mathrm{in}}}^\infty \frac{\nu\mathrm{d}\nu}{\sqrt{P_5^\vartheta(\nu)}}\right)^T. \tag{39}$$

C. ϕ equation

We need to use Eqs. (9) and (10) to rewrite the ϕ equation (11) in the form

$$\mathrm{d}\phi = \frac{\tilde{a}\,\tilde{\Xi}(\tilde{B}E - \tilde{a}\,\tilde{L}\,\tilde{\Xi})}{\tilde{R}}\frac{\mathrm{d}\tilde{r}}{\sqrt{X}} + \frac{\tilde{\Xi}(\tilde{A}E - \tilde{L}\,\tilde{\Xi})}{\tilde{\Theta}\sin\vartheta}\frac{\mathrm{d}\vartheta}{\sqrt{Y}} \tag{40}$$

and in integral form

$$\begin{aligned}\phi - \phi_{\mathrm{in}} = &\int_{\tilde{r}_{\mathrm{in}}}^{\tilde{r}} \frac{\tilde{a}\,\tilde{\Xi}(\tilde{B}E - \tilde{a}\,\tilde{L}\,\tilde{\Xi})}{\tilde{R}}\frac{\mathrm{d}\tilde{r}}{\sqrt{X}} \\ &+ \int_{\vartheta_{\mathrm{in}}}^{\vartheta} \frac{\tilde{\Xi}(\tilde{A}E - \tilde{L}\,\tilde{\Xi})}{\tilde{\Theta}\sin\vartheta}\frac{\mathrm{d}\vartheta}{\sqrt{Y}} = I_{\tilde{r}}(\tilde{r}) + I_\vartheta(\vartheta).\end{aligned} \tag{41}$$

$I_{\tilde{r}}$ and I_ϑ can be solved separately.

1. Elliptic case

Again, in the case of $\tilde{g} = 0$ or $\delta = 0$, the solution is much simpler. We start with the $\tilde{r}$-dependent integral $I_{\tilde{r}}$ and substitute $\tilde{r} = \pm\frac{b_3}{4y - \frac{b_2}{3}} + \tilde{r}_X$ and apply a partial fraction decomposition,

$$I_{\tilde{r}} = \int_{y_{\mathrm{in}}}^{y}\left(C_0 + \sum_{i=1}^{2}\frac{C_i}{y' - p_i}\right)\frac{\mathrm{d}y'}{\sqrt{P_3^{\tilde{r}}(y')}}, \tag{42}$$

where C_i are constants which arise from the partial fraction decomposition and p_i are first-order poles of $I_{\tilde{r}}$. With the last substitution $y = \wp(v'; g_2^{\tilde{r}}, g_3^{\tilde{r}}) = \wp_{\tilde{r}}(v')$, where $v' = \gamma - \gamma'_{\mathrm{in}}$, we get

$$I_{\tilde{r}} = \int_{v'_{\mathrm{in}}}^{v'}\left(C_0 + \sum_{i=1}^{2}\frac{C_i}{\wp_{\tilde{r}}(v') - p_i}\right)\mathrm{d}v'. \tag{43}$$

The ϑ-dependent integral I_ϑ can be stated in a similar form with the substitution $\cos\vartheta = \pm\frac{b_3'}{4\wp_\vartheta(v'') - \frac{b_2'}{3}} + \nu_y$,

$$I_\vartheta = \int_{v''_{\mathrm{in}}}^{v'}\left(C_0' + \sum_{i=1}^{2}\frac{C_i'}{\wp_\vartheta(v'') - p_i'}\right)\mathrm{d}v'', \tag{44}$$

where C_i' are the corresponding constants from the partial fraction decomposition and p_i' are the first-order poles of I_ϑ and $\wp_\vartheta(v'') = \wp(v''; g_2^\vartheta, g_3^\vartheta)$, with $v'' = \gamma - \gamma''_{\mathrm{in}}$. Both integrals are third kind elliptic integrals and can be solved in terms of the Weierstraß $\wp$, σ, and ζ functions (see Ref. [11,12,23]). Therefore, we can state the solution of Eq. (11) as

$$\begin{aligned}\phi(\gamma) - \phi_{\mathrm{in}} = &\, C_0(v' - v'_{\mathrm{in}}) + \sum_{i=1}^{2}\left(2\zeta_{\tilde{r}}(v_i')(v' - v'_{\mathrm{in}}) + \ln\frac{\sigma_{\tilde{r}}(v' - v_i')}{\sigma_{\tilde{r}}(v'_{\mathrm{in}} - v_i')} - \ln\frac{\sigma_{\tilde{r}}(v' + v_i')}{\sigma_{\tilde{r}}(v'_{\mathrm{in}} + v_i')}\right) \\ &\times C_0'(v'' - v''_{\mathrm{in}}) + \sum_{i=1}^{2}\left(2\zeta_\vartheta(v_i'')(v'' - v''_{\mathrm{in}}) + \ln\frac{\sigma_\vartheta(v'' - v_i'')}{\sigma_\vartheta(v''_{\mathrm{in}} - v_i'')} - \ln\frac{\sigma_\vartheta(v'' + v_i'')}{\sigma_\vartheta(v''_{\mathrm{in}} + v_i'')}\right),\end{aligned} \tag{45}$$

with $p_i = \wp_{\tilde{r}}(v_i')$, $p_i = \wp_\vartheta(v_i'')$ and

$$\begin{aligned}&\wp_{\tilde{r}}(v) = \wp(v, g_2^{\tilde{r}}, g_3^{\tilde{r}}), \qquad \wp_\vartheta(v) = \wp(v, g_2^\vartheta, g_3^\vartheta), \\ &\zeta_{\tilde{r}}(v) = \zeta(v, g_2^{\tilde{r}}, g_3^{\tilde{r}}), \qquad \zeta_\vartheta(v) = \zeta(v, g_2^\vartheta, g_3^\vartheta), \\ &\sigma_{\tilde{r}}(v) = \sigma(v, g_2^{\tilde{r}}, g_3^{\tilde{r}}), \qquad \sigma_\vartheta(v) = \sigma(v, g_2^\vartheta, g_3^\vartheta).\end{aligned} \tag{46}$$

2. Hyperelliptic case

For the full solution, we can write the integrals $I_{\tilde{r}}$ and I_ϑ in a form like

$$I = \int_{x_{\mathrm{in}}}^{x}\frac{\mathrm{d}x'}{(x - Z)\sqrt{P_5(x)}}, \tag{47}$$

where $P_5(x)$ is a polynomial of fifth order in x and Z is a pole. This is a hyperelliptic integral of the third kind, and following Ref. [23], it can be solved by

$$\begin{aligned}I = &\frac{2}{\sqrt{P_5(Z)}}\int_{x_{\mathrm{in}}}^{x}\mathrm{d}\vec{z}^T\int_{e_2}^{Z}\mathrm{d}\vec{y} + \ln\left(\frac{\sigma(\int_\infty^x \mathrm{d}\vec{z} - \int_{e_2}^Z \mathrm{d}\vec{z})}{\sigma(\int_\infty^x \mathrm{d}\vec{z} + \int_{e_2}^Z \mathrm{d}\vec{z})}\right) \\ &- \ln\left(\frac{\sigma(\int_\infty^{x_{\mathrm{in}}} \mathrm{d}\vec{z} - \int_{e_2}^Z \mathrm{d}\vec{z})}{\sigma(\int_\infty^{x_{\mathrm{in}}} \mathrm{d}\vec{z} + \int_{e_2}^Z \mathrm{d}\vec{z})}\right),\end{aligned} \tag{48}$$

where e_2 is a zero of $P_5(x)$ and

$$\mathrm{d}\vec{z} := \left(\frac{\mathrm{d}x}{\sqrt{P_5(x)}}, \frac{x\mathrm{d}x}{\sqrt{P_5(x)}}\right)^T \tag{49}$$

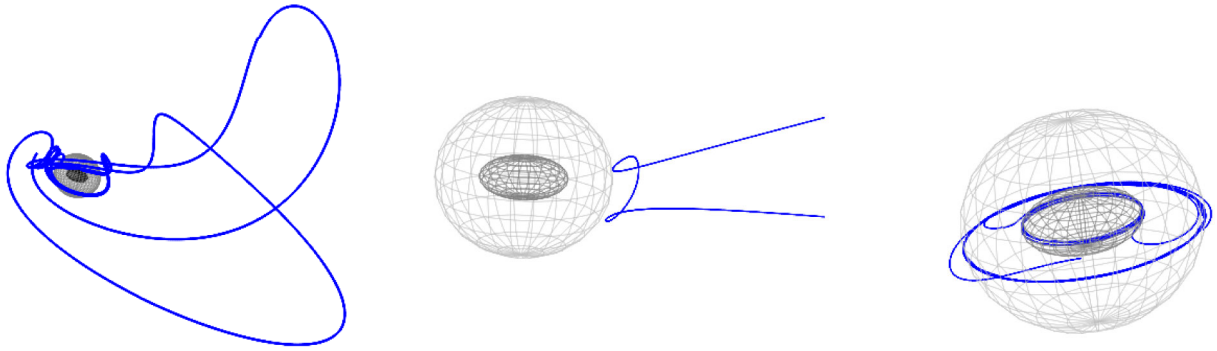

(a) $\delta = 1$, $\tilde{a} = -0.4$, $\tilde{g} = 0.2$, $\tilde{N}_g = -0.07$, $\tilde{e} = 0.07$, $\tilde{v} = 1.2$, $\tilde{K} = -0.1$, $\tilde{L} = -1$, $E = 2.8$: Bound orbit

(b) $\delta = 1$, $\tilde{a} = 0.4$, $\tilde{g} = 0$, $\tilde{N}_g = 0$, $\tilde{e} = 0$, $\tilde{v} = 0$, $\tilde{K} = -10$, $\tilde{L} = 2.3$, $E = 1.953$: Escape Orbit

(c) $\delta = 1$, $\tilde{a} = 0.4$, $\tilde{g} = 0$, $\tilde{N}_g = 0$, $\tilde{e} = 0$, $\tilde{v} = 0$, $\tilde{K} = -10$, $\tilde{L} = 2.3$, $E = 1.953$: Many-world bound orbit

FIG. 6. Orbits of test particles in the dyonic rotating black hole spacetime. The orbit is represented by the blue line, and the outer and inner horizons are denoted by gray and black ellipsoids.

$$\mathrm{d}\vec{y} = \left(\sum_{k=1}^{4} k a_{k+1} \frac{x^k \mathrm{d}x}{4\sqrt{P_5(x)}}, \sum_{k=2}^{3} (k-1) a_{k+3} \frac{x^k \mathrm{d}x}{4\sqrt{P_5(x)}}\right)^T \tag{50}$$

are holomorphic and meromorphic differentials. Here, a_k denote the coefficients of the polynomial $P_5(x)$.

D. $\tilde{t}$ equation

The $\tilde{t}$ equation (12) can be solved analogously to the ϕ equation (11) and has solutions of the form of Eq. (45) for $\tilde{g} = 0$ or $\delta = 0$ or of the form of Eq. (48) for the full solution.

V. ORBITS

Now, we can use the analytical solutions to visualize the possible orbits in this spacetime. In Fig. 6, examples of a bound orbit, an escape orbit, and a many-world bound orbit are shown. Figure 6(a) shows the special case of a zoom-whirl orbit, where the particle makes several turns near the horizon, then escapes to a region far away from the black hole and turns back to the near-horizon regime. Figure 7(a) shows a BO which lies inside the singularity. We cut out a part of the ringoid structure to make it visible. The orbit in Fig. 7(b) shows an escape orbit around a naked singularity for negative $\tilde{r}$. The singularity has a toroidal form, and it may be possible to fly through the hole in the middle. The last orbit in Fig. 7(c) shows a two-world escape orbit, where the turning point is very close to the inner horizon. The singularity for this black hole is an ellipsoid.

VI. CONCLUSION

In this paper, we derived the equations of motion for test particles and light in the $\mathrm{U}(1)^2$ dyonic rotating black hole

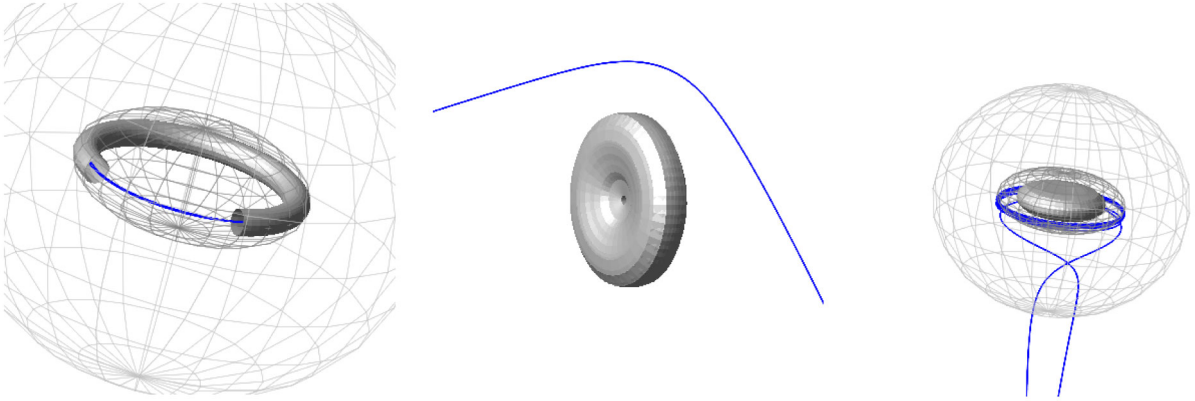

(a) $\delta = 1$, $\tilde{a} = -0.4$, $\tilde{g} = 0$, $\tilde{N}_g = 0$, $\tilde{e} = 0$, $\tilde{v} = 0.2$, $\tilde{K} = -1$, $\tilde{L} = 4.6$, $E = 12$: Bound orbit

(b) $\delta = 1$, $\tilde{a} = 0.3$, $\tilde{g} = 0$, $\tilde{N}_g = 0.2$, $\tilde{e} = 0.2$, $\tilde{v} = 0.1$, $\tilde{K} = -0.1$, $\tilde{L} = 3$, $E = 4$: Escape orbit with $\tilde{r} < 0$

(c) $\delta = 1$, $\tilde{a} = 0.4$, $\tilde{g} = 0$, $\tilde{N}_g = 0.35$, $\tilde{e} = 0.35$, $\tilde{v} = 0.1$, $\tilde{K} = 0.1$, $\tilde{L} = 3$, $E = 2$: Two-world escape orbit

FIG. 7. Orbits of test particles in the dyonic rotating black hole spacetime. The orbit is represented by the blue line, and the outer and inner horizons are denoted by gray and black ellipsoids. The gray structure denotes the singularity.

spacetime and stated their analytical solution in two cases. For the full solution, we had to use methods for solving hyperelliptic differential equations of the first and third kinds. For a vanishing gauge coupling constant or light, the solution can be formulated in an easier form, since we only had to solve elliptic differential equations. We were able to characterize the possible orbit types for two-horizon black holes. These were orbits we already know from the special cases of the spacetimelike escape orbits and bound orbits. A special feature are bound orbits and many-world bound orbits, which cross $\tilde{r} = 0$. We call these CBO or CMBO. In addition, we found an interesting structure of the singularity varying from toruslike structures to ellipsoids for $\tilde{r} \geq 0$ in contrast to the EMDA black hole [16].

Future work could be the characterization of geodesic motion for black holes with more than two horizons, especially the influence of the negative valued horizon on the particle motion. Another step is to derive the equations of motion for charged particles or to consider an even more general black hole with more charges. In these cases, we have to deal with hyperelliptic integrals of genus bigger than 2 or even more complicated differential equations. The analytical solutions we derived can now be used to calculate observables like the periastron shift, the light deflection, or the shadow of the black hole, which eventually can be compared to observations in the future.

ACKNOWLEDGMENTS

We would like to thank Jutta Kunz for helpful and interesting discussions. S. G. gratefully acknowledges support by the DFG, within the Research Training Group *Models of Gravity.*

[1] J. M. Maldacena, Adv. Theor. Math. Phys. **2**, 231 (1998).
[2] S. Matarrese, M. Colpi, V. Gorini, and U. Moschella (eds.), *Dark Matter and Dark Energy*, Astrophysics and Space Science Library (Springer, Berlin, 2011), Vol. 370.
[3] F. S. Guzman and T. Matos, Classical Quantum Gravity **17**, L9 (2000).
[4] D. D. K. Chow and G. Compère, Phys. Rev. D **89**, 065003 (2014).
[5] E. Lozano-Tellechea and T. Ortin, Nucl. Phys. **B569**, 435 (2000).
[6] A. Garcia, D. Galtsov, and O. Kechkin, Phys. Rev. Lett. **74**, 1276 (1995).
[7] B. Carter, Commun. Math. Phys. **10**, 280 (1968).
[8] M. Walker and R. Penrose, Commun. Math. Phys. **18**, 265 (1970).
[9] Y. Chervonyi and O. Lunin, J. High Energy Phys. 09 (2015) 182.
[10] Y. Hagihara, Jpn. J. Astron. Geophys. **8**, 67 (1931).
[11] V. Kagramanova, J. Kunz, E. Hackmann, and C. Lämmerzahl, Phys. Rev. D **81**, 124044 (2010).
[12] S. Grunau and V. Kagramanova, Phys. Rev. D **83**, 044009 (2011).
[13] V. Kagramanova and S. Reimers, Phys. Rev. D **86**, 084029 (2012).
[14] E. Hackmann and H. Xu, Phys. Rev. D **87**, 124030 (2013).
[15] H. Cebeci, N. Özdemir, and S. Şentorun, Phys. Rev. D **93**, 104031 (2016).
[16] K. Flathmann and S. Grunau, Phys. Rev. D **92**, 104027 (2015).
[17] A. Sen, Phys. Rev. D **69**, 1006 (1992).
[18] E. Hackmann and C. Lämmerzahl, Phys. Rev. Lett. **100**, 171101 (2008).
[19] E. Hackmann and C. Lämmerzahl, Phys. Rev. D **78**, 024035 (2008).
[20] E. Hackmann, V. Kagramanova, J. Kunz, and C. Lämmerzahl, Phys. Rev. D **78**, 124018 (2008); **79**, 029901(E) (2009).
[21] E. Hackmann, C. Lämmerzahl, V. Kagramanova, and J. Kunz, Phys. Rev. D **81**, 044020 (2010).
[22] V. Z. Enolski, E. Hackmann, V. Kagramanova, J. Kunz, and C. Lämmerzahl, J. Geom. Phys. **61**, 899 (2011).
[23] V. Enolski, B. Hartmann, V. Kagramanova, J. Kunz, C. Lämmerzahl, and P. Sirimachan, J. Math. Phys. (N.Y.) **53**, 012504 (2012).
[24] S. Soroushfar, R. Saffari, J. Kunz, and C. Lämmerzahl, Phys. Rev. D **92**, 044010 (2015).
[25] S. Soroushfar, R. Saffari, and S. Grunau, arXiv:1605.08975.
[26] B. Carter, Phys. Rev. **174**, 1559 (1968).
[27] Y. Mino, Phys. Rev. D **67**, 084027 (2003).
[28] A. I. Markushevich, *Theory of Functions of a Complex Variable* (Prentice-Hall, Englewood Cliffs, NJ, 1967), Vol. III.
[29] E. Hackmann and C. Lämmerzahl, Phys. Rev. **100**, 171101 (2008).